



Physicochemical and thermodynamic properties of aqueous blends of 3-aminopropyl triethoxysilane and amines at 298.15–333.15 K

Sweta Balchandani^{a,b}, Bishnupada Mandal^{a,*}, Sahil Garg^{c,*}, Mengran Li^{c,*}, Swapnil Dharaskar^b

^a Department of Chemical Engineering, Indian Institute of Technology Guwahati, Guwahati 781039, India

^b CO₂ research group, Department of Chemical Engineering, Pandit Deendayal Petroleum University, Gandhinagar 382007, India

^c School of Chemical Engineering, The University of Queensland, St Lucia 4072, Australia

ARTICLE INFO

Article history:

Received 11 October 2020

Received in revised form 7 January 2021

Accepted 18 January 2021

Available online 24 January 2021

Keywords:

Density

Viscosity

Sound velocity

Refractive index

Blended-amines

ABSTRACT

We report the density, viscosity, sound velocity, and refractive index experimental data of four silane–amine blended systems viz. (1) 3-aminopropyl triethoxysilane (TESA) + N-(2-aminoethyl) piperazine (AEP), (2) 3-aminopropyl triethoxysilane (TESA) + 2-methyl-1-propanol (AMP) (3) 3-aminopropyl triethoxysilane (TESA) + Methyl-diethanolamine (MDEA) and (4) 3-aminopropyl triethoxysilane (TESA) + Diethanolamine (DEA). The temperature range for all the measurements is (298.15–333.15) K up to a mole fraction of 0.2 of TESA in the solution. The physicochemical properties were well fitted against the first principle and artificial neural network models. We further calculated key properties for CO₂ capture such as diffusivity in CO₂, isentropic compressibility, thermal expansion coefficients, Gibb's free energy, entropy, and enthalpy of activation. The data collected from this work could contribute to further detailed kinetic analysis of CO₂ absorption over these capturing solvents

© 2021 Elsevier B.V. All rights reserved.

1. Introduction

Carbon dioxide is considered to be one of the major contributors to global greenhouse gas emissions. Absorption-regeneration technology aided with various improved solvents is a promising approach towards the mitigation of carbon dioxide. The conventional solvents such as monoethanolamine (MEA), diethanolamine (DEA), N-methyldiethanolamine (MDEA) poses various drawbacks such as high solvent loss and degradation, equipment corrosion, and higher regeneration energy requirement, making the process inefficient and economically unfavorable [1,2]. To overcome these limitations, novel solvents such as ionic liquids (IL) can be considered as a potential solvent for gas sweetening technology. Ionic liquid possesses many favorable features such as negligible vapor pressure which reduces the solvent losses to the environment. Other unique properties of IL include its high thermal stability, higher conductivity, non-flammability as well as ease of separation since it requires very less regeneration energy, and it possesses reversible and phase changing behaviors [3].

Despite its various advantages, the applicability of ILs as solvents for acid gas separation is limited because of their high cost and lower CO₂ absorption rate. Hence, the application of a hybrid solvent such as a

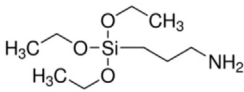
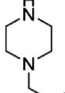
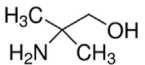
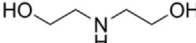
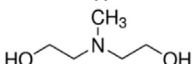
mixture of (alkanolamine + IL) or functionalized IL can be explored as an alternative solvent since it combines the advantages of both the solvents [4,5]. While functionalized ILs have better capacities than the pure ILs or mixture of ILs + amine, but they have high viscosity and require advanced purification steps in the synthesis process, which makes the overall process of CO₂ capture economically infeasible.

Recently, reversible solvents are emerging as a promising candidate for CO₂ capture. They can switch between a solvent that is either ionic or non-ionic. Taking silylamine-based solvent as an example, it serves as a non-ionic solvent to absorb CO₂ chemically to form a reversible ionic liquid (RevIL), which can further absorb CO₂ physically in an ionic form [6]. Such CO₂-rich solvent can switch back to CO₂-lean non-ionic solvents upon heating [7]. The reversible solvents normally show lower viscosity than conventional ILs because of the bond lengthening in the silylated derivatives and intermolecular interactions in the ionic form [6]. The reversible solvents stand out because of their high capacity of CO₂ absorption over nitrogen (N₂) in dilute flue gas streams [6,8–11]. In addition, the total quantity of solvent required can be drastically reduced compared to conventional alkanolamine solvents. For example, Blasucci et al. [6] has investigated the efficiency of 3-aminopropyl triethoxysilane (TESA) as a reversible solvent for CO₂ capture processes. Their thermophysical properties have been reported such as solvent densities, viscosities, thermal stability as well as total CO₂ capture capacities (14.76 mol of CO₂/kg of amine) at 35 °C and 62.5 bar is much higher than in 30 wt% DEA solutions. Another example is the

* Corresponding authors.

E-mail addresses: bpmandal@iitg.ac.in (B. Mandal), sahil.garg@uq.edu.au (S. Garg), m.li6@uq.edu.au (M. Li).

Table 1
Specification of the Chemicals used in the present work.

Chemical Name	Structure	Molecular weight kg.kmol ⁻¹	Source	Purity (%)	CAS no.	Purification method
3-aminopropyl triethoxysilane (TESA)		221.37	Sigma Aldrich	99	919-30-2	None
1-(2-Aminoethyl) Piperazine (AEP)		129.21	Sigma Aldrich	99	140-31-8	None
2-Amino-2-Methyl-1-Propanol (AMP)		89.14	Sigma Aldrich	99	124-68-5	None
Diethanolamine (DEA)		105.14	Sigma Aldrich	>98	111-42-2	None
N-Methyldiethanolamine (MDEA)		119.163	Sigma Aldrich	99	105-59-9	None

COSMO-RS studies by Gonzalez-Miquel et al. [9], who reported that the RevILs have a stronger capacity for CO₂ physisorption and require lower energy for solvent regeneration when compared with MEA solutions.

Recently, Madden et al. (2016) [8] studied the efficiency of silane functionalized adsorbent for CO₂ capture, and reported that simple post-synthesis addition of aminopropyl triethoxysilane to amine co-condensed silica increases the uptake of CO₂ to 211 mg CO₂ g⁻¹ at 35 °C. Recent research efforts have investigated the efficiency of amines

such as AEP [12], AMP [13], MDEA [14], and DEA [15]. Recent studies [16–19] also highlight the importance of understanding the physico-chemical properties of various applied solvents such as ionic liquids blended with amines. A combination of TESA with all the above-mentioned amines hold promise as potential solvents for CO₂ absorption. Knowing the physicochemical properties such as density, viscosity, surface tension, the refractive index is also essential for the rational design of the absorption column. These data also play a major role in the

Table 2
Experimental Densities (ρ), Dynamic Viscosity (η), Kinematic Viscosity (ν), Sound Velocity (c) and Refractive Index (n_D) for TESA (1) + AEP (2) + H₂O (3) from 298.15 K to 333.15 K at 0.1 MPa.^a

	T/K	298.15	303.15	308.15	313.15	318.15	323.15	328.15	333.15
	x_1	TESA (1) + AEP (2) + H ₂ O (3)							
$\rho/\text{kg.m}^{-3}$	0.0474	1027.4	1022.6	1017.9	1012.6	1008.0	1003.5	998.9	994.4
	0.0724	1019.9	1015.4	1010.9	1006.5	1002.1	997.5	992.7	987.5
	0.0982	1014.9	1010.3	1005.6	1000.9	996.2	991.5	984.9	979.6
	0.1249	1007.5	1002.4	997.9	991.7	987.0	982.3	976.6	971.9
	0.1526	998.1	992.8	987.1	982.1	977.3	972.5	968.1	961.1
$\eta/\text{mPa.s}$	0.1813	989.9	985.3	980.3	974.7	969.8	964.1	955.8	941.8
	0.0474	159.81	113.69	84.02	62.90	49.53	38.49	30.45	24.53
	0.0724	136.40	99.32	74.18	56.44	43.89	34.67	27.82	22.66
	0.0982	99.30	75.36	57.88	45.19	35.83	28.87	23.56	19.46
	0.1249	83.02	64.23	50.59	40.41	32.65	26.67	22.01	18.39
ν/cS	0.1526	66.47	52.57	42.20	34.23	28.07	23.24	19.48	16.48
	0.1813	53.15	43.15	35.16	29.05	24.13	20.25	17.18	14.71
	0.0474	155.56	111.18	82.54	62.12	49.14	38.36	30.48	24.67
	0.0724	133.73	97.82	73.38	56.07	43.81	34.76	28.03	22.94
	0.0982	97.83	74.59	57.55	45.15	35.97	29.11	23.92	19.86
$c/\text{m.s}^{-1}$	0.1249	82.41	64.08	50.69	40.74	33.07	27.15	22.54	18.93
	0.1526	66.59	52.95	42.75	34.85	28.72	23.89	20.12	17.15
	0.1813	53.68	43.79	35.87	29.79	24.88	21.01	17.97	15.62
	0.0474	1719.8	1701.7	1683.4	1664.7	1645.9	1626.7	1607.7	1607.1
	0.0724	1673.4	1655.9	1638.2	1620.1	1601.5	1582.8	1565.2	1547.5
n_D	0.0982	1606.8	1590.4	1573.9	1557.1	1540.3	1523.7	1506.7	1489.5
	0.1249	1550.7	1534.8	1518.7	1502.4	1486.0	1469.9	1453.3	1436.6
	0.1526	1492.3	1476.9	1461.3	1445.5	1429.6	1413.8	1397.7	1381.5
	0.1813	1434.5	1419.3	1404.0	1388.6	1373.0	1357.6	1341.8	1325.8
	1.0	1230.6	1212.2	1193.7	1175.4	1157.2	1139.1	1121.5	1103.8
n_D	0.0474	1.460	1.459	1.457	1.455	1.454	1.453	–	–
	0.0724	1.453	1.451	1.449	1.447	1.446	1.444	–	–
	0.0982	1.443	1.441	1.442	1.438	1.438	1.437	–	–
	0.1249	1.434	1.434	1.431	1.429	1.429	1.427	–	–
	0.1526	1.424	1.422	1.420	1.419	1.418	1.418	–	–
	0.1813	1.413	1.411	1.410	1.408	1.408	1.407	–	–

^a The standard uncertainties u (0.68 level of confidence) are $u(T) = 0.01$ K, $u(P) = 0.2$ kPa, $u(\rho) = 0.50$ kg·m⁻³, $u(\eta) = 0.07$ mPa.s, $u(\nu) = 0.09$ cS, $u(n_D) = 0.001$, $u(c) = 0.5$ m.s⁻¹, $u(x) = 0.0001$.

Table 3Experimental Densities (ρ), Dynamic Viscosity (η), Kinematic Viscosity (ν), Sound Velocity (c) and Refractive Index (nD) for TESA (1) + AMP (2) + H₂O (3) from 298.15 K to 333.15 K at 0.1 MPa.^a

	T/K	298.15	303.15	308.15	313.15	318.15	323.15	328.15	333.15
	x_1	TESA (1) + AMP (2) + H ₂ O (3)							
$\rho/\text{kg.m}^{-3}$	0.0431	977.8	973.7	969.5	965.4	961.2	956.9	952.6	948.3
	0.0668	980.3	976.1	971.9	967.6	963.4	959.0	954.6	949.9
	0.0921	981.6	977.9	973.4	969.7	965.1	960.6	955.3	947.9
	0.1192	983.4	978.4	975.5	969.9	966.1	961.7	956.9	951.0
	0.1483	984.1	979.4	972.9	968.3	962.7	957.9	950.2	940.7
$\eta/\text{mPa.s}$	0.1795	988.3	983.2	976.9	970.8	966.8	960.1	950.7	934.9
	0.0431	64.25	48.64	37.66	29.65	23.74	19.29	15.97	13.44
	0.0668	60.13	46.39	36.44	29.04	23.46	19.20	15.98	13.52
	0.0921	54.20	42.50	33.86	27.34	22.37	18.54	15.56	13.25
	0.1192	51.52	40.84	32.76	26.38	21.53	17.92	15.21	13.08
ν/cS	0.1483	48.74	39.23	31.91	29.62	21.78	18.26	15.50	13.31
	0.1795	49.26	39.79	32.49	26.39	22.29	18.77	15.96	13.68
	0.0431	65.71	49.95	38.84	30.72	24.70	20.16	16.77	14.17
	0.0668	61.35	47.53	37.49	30.01	24.35	20.02	16.75	14.23
	0.0921	55.22	43.46	34.78	28.19	23.18	19.30	16.29	13.98
$c/\text{m.s}^{-1}$	0.1192	52.39	41.74	33.58	27.19	22.28	18.63	15.89	13.75
	0.1483	49.53	40.05	32.79	40.89	22.62	19.06	16.31	14.15
	0.1795	49.84	40.47	33.25	27.59	23.06	19.55	16.79	14.63
	0.0431	1597.6	1582.0	1566.2	1550.2	1534.2	1518.3	1502.0	1485.4
	0.0668	1550.1	1535.0	1519.3	1503.5	1488.0	1472.0	1455.8	1439.4
nD	0.0921	1517.6	1502.4	1486.9	1471.4	1455.6	1440.1	1424.1	1407.9
	0.1192	1496.0	1486.0	1465.8	1445.7	1400.1	1399.5	1385.7	1374.2
	0.1483	1453.8	1438.4	1422.9	1407.8	1392.2	1376.4	1360.4	1344.3
	0.1795	1423.7	1408.5	1393.2	1377.8	1362.5	1346.9	1331.2	1315.3
	1.0	1230.6	1212.2	1193.7	1175.4	1157.2	1139.1	1121.5	1103.8
nD	0.0431	1.421	1.419	1.417	1.416	1.413	1.413	–	–
	0.0668	1.419	1.418	1.416	1.415	1.412	1.411	–	–
	0.0921	1.417	1.415	1.413	1.412	1.411	1.409	–	–
	0.1192	1.415	1.413	1.412	1.411	1.411	1.409	–	–
	0.1483	1.412	1.410	1.408	1.408	1.407	1.404	–	–
	0.1795	1.409	1.409	1.407	1.406	1.406	1.404	–	–

^a The standard uncertainties u (0.68 level of confidence) are $u(T) = 0.01$ K, $u(P) = 0.2$ kPa, $u(\rho) = 0.50$ kg·m⁻³, $u(\eta) = 0.07$ mPa.s, $u(\nu) = 0.09$ cS, $u(nD) = 0.001$, $u(c) = 0.5$ m.s⁻¹, $u(x) = 0.0001$.

Table 4Experimental Densities (ρ), Dynamic Viscosity (η), Kinematic Viscosity (ν), Sound Velocity (c) and Refractive Index (nD) for TESA (1) + DEA (2) + H₂O (3) from 298.15 K to 333.15 K at 0.1 MPa.^a

	T/K	298.15	303.15	308.15	313.15	318.15	323.15	328.15	333.15
	x_1	TESA (1) + DEA (2) + H ₂ O (3)							
$\rho/\text{kg.m}^{-3}$	0.0451	1056.9	1053.5	1050.1	1046.5	1042.9	1039.2	1035.5	1031.7
	0.0694	1045.6	1042.0	1038.4	1034.7	1030.9	1027.1	1023.2	1019.3
	0.0950	1032.1	1028.4	1024.6	1020.8	1016.8	1012.9	1008.8	1004.7
	0.1219	1019.9	1015.9	1011.9	1007.9	1003.8	999.7	995.4	991.2
	0.1504	1006.9	1002.8	998.7	994.5	990.1	985.6	980.6	974.0
$\eta/\text{mPa.s}$	0.1804	993.5	988.2	983.8	977.6	972.3	967.1	959.3	944.7
	0.0451	116.39	88.44	68.57	53.99	43.17	34.94	28.61	23.76
	0.0694	100.81	77.44	60.54	48.19	38.79	31.70	26.17	21.82
	0.0950	84.16	65.67	51.95	41.70	33.90	27.83	23.20	19.54
	0.1219	69.02	55.08	44.29	35.94	29.50	24.48	20.49	17.36
ν/cS	0.1504	61.87	49.69	40.16	32.89	27.14	22.69	19.09	16.29
	0.1804	48.71	39.95	32.75	27.14	22.68	19.12	16.29	14.01
	0.0451	110.11	83.95	65.30	51.59	41.39	33.62	27.63	23.04
	0.0694	96.41	74.32	58.31	46.58	37.63	30.86	25.58	21.41
	0.0950	81.54	63.85	50.70	40.85	33.34	27.48	22.99	19.45
$c/\text{m.s}^{-1}$	0.1219	67.68	54.21	43.77	35.66	29.39	24.49	20.59	17.52
	0.1504	61.45	49.56	40.21	33.08	27.41	23.02	19.47	16.72
	0.1804	49.03	40.42	33.29	27.77	23.32	19.77	16.99	14.84
	0.0451	1687.1	1674.5	1662.0	1649.7	1637.0	1624.1	1611.0	1597.7
	0.0694	1633.4	1620.7	1607.8	1594.7	1581.7	1568.3	1554.7	1541.0
nD	0.0950	1580.0	1566.5	1553.0	1539.7	1526.1	1512.2	1498.2	1484.0
	0.1219	1530.6	1516.7	1502.8	1488.7	1474.5	1460.3	1445.8	1430.9
	0.1504	1478.4	1464.0	1449.9	1435.4	1420.8	1406.0	1391.2	1376.0
	0.1804	1436.9	1421.8	1407.1	1392.4	1377.3	1362.2	1346.8	1331.3
	1.0	1230.6	1212.2	1193.7	1175.4	1157.2	1139.1	1121.5	1103.8
nD	0.0451	1.433	1.432	1.430	1.429	1.429	1.427	–	–
	0.0694	1.429	1.429	1.427	1.426	1.426	1.426	–	–
	0.0950	1.425	1.424	1.422	1.420	1.419	1.418	–	–
	0.1219	1.421	1.419	1.418	1.417	1.416	1.416	–	–
	0.1504	1.417	1.416	1.414	1.412	1.411	1.411	–	–
	0.1804	1.411	1.409	1.408	1.407	1.406	1.407	–	–

^a The standard uncertainties u (0.68 level of confidence) are $u(T) = 0.01$ K, $u(P) = 0.2$ kPa, $u(\rho) = 0.50$ kg·m⁻³, $u(\eta) = 0.07$ mPa.s, $u(\nu) = 0.09$ cS, $u(nD) = 0.001$, $u(c) = 0.5$ m.s⁻¹, $u(x) = 0.0001$.

detailed kinetic analysis of CO₂ absorption processes [20–22]. This work focuses on the determination of physicochemical properties such as density, viscosity, refractive index, and sound velocity of ternary aqueous mixtures of (TESA + AEP), (TESA + AMP), (TESA + DEA), and (TESA + MDEA) in the temperature range of 298.15–333.15 K. Two first principles and one artificial neural network models were applied to correlate the experimental data in this work. We also estimated key properties of the blends such as CO₂ diffusivity and thermodynamic properties such as Gibbs energy, enthalpy, and entropy of activation of viscous flow at the same temperature ranges.

2. Experimental section

2.1. Chemicals

Detailed specifications of the chemicals used in the present work are specified in Table 1. All chemicals were of analytical grade and used without further purification.

2.2. Sample preparation

Different blends based on mole fractions for the ternary aqueous mixture of (TESA + AEP), (TESA + AMP), (TESA + DEA), and (TESA + MDEA) were prepared using Milipore® water. The samples were measured using METTLER TOLEDO (JB1603-C/FACT) carat balance with an uncertainty of 0.0001 g. The samples were stirred sufficiently to ensure proper mixing and uniformity in the solvents.

2.3. Apparatus and procedure

The detailed description and the accuracy of the adopted methodology about the measurements of density, viscosity, sound velocity, and

refractive index are reported in our previous work [23,24]. Only brief details are presented here. Density and sound velocity, viscosity and refractive index measurements of the ternary mixtures were carried out with density and sound velocity meter (DSA 5000 M, Anton Paar, Austria), Anton Paar AMVn rolling ball viscometer, and METTLER TOLEDO RE40 refractometer, correspondingly. All the measurements were carried out in the temperature range of (298.15–333.15) K. The standard uncertainties, u , are as follows: temperature: $u(T) = 0.01$ K, pressure: $u(P) = 0.2$ kPa, density: $u(\rho) = 0.5 \text{ kg} \cdot \text{m}^{-3}$, sound velocity: $u(c) = 0.5 \text{ m} \cdot \text{s}^{-1}$, viscosity: $u(\eta) = 0.07 \text{ mPa} \cdot \text{s}$, refractive index: $u(nD) = 0.001$.

3. Results and discussion

The measured densities, ρ , viscosities, μ , refractive index, nD , and the sound velocity, c for the ternary aqueous mixtures of TESA with AEP, AMP, DEA, and MDEA at $T = (298.15, 303.15, 308.15, 313.15, 318.15, 323.15, 328.15, \text{ and } 333.15) \text{ K}$ within the overall composition range are listed in Tables 2, 3, 4 and 5.

3.1. Density

The experimental density results, as shown in Fig. 1, indicate that the densities of all the tested aqueous TESA - amine mixtures all increase with temperature at 298.15–333.15 K. Such dependency on temperature is due to the weakened intermolecular attraction forces that increase the space amid the solvent molecules and thereby the overall volume of the solvents. Interestingly, the mole fraction of TESA also plays a role in determining the overall solvent density. As shown in Fig. 1(a, c, d), increasing TESA concentration lowers the densities of aqueous (TESA + AEP), (TESA + DEA), and (TESA + MDEA). In

Table 5

Experimental Densities (ρ), Dynamic Viscosity (η), Kinematic Viscosity (ν), Sound Velocity (c) and Refractive Index (nD) for TESA (1) + MDEA (2) + H₂O (3) from 298.15 K to 333.15 K at 0.1 MPa.^a

	T/K	298.15	303.15	308.15	313.15	318.15	323.15	328.15	333.15
	x_1	TESA (1) + MDEA (2) + H ₂ O (3)							
$\rho/\text{kg} \cdot \text{m}^{-3}$	0.0466	1033.4	1029.2	1025.1	1020.9	1016.7	1012.2	1007.7	1003.1
	0.0712	1026.7	1022.6	1018.5	1014.3	1010.0	1005.7	1001.0	995.8
	0.0970	1017.9	1013.7	1009.5	1005.2	1000.8	996.2	991.0	984.8
	0.1238	1009.7	1005.4	1001.1	996.6	992.1	987.1	981.2	973.4
	0.1518	1001.3	996.7	991.6	985.9	980.4	973.6	966.5	954.8
	0.1810	992.5	987.9	983.0	977.7	972.4	966.2	959.0	942.9
$\eta/\text{mPa} \cdot \text{s}$	0.0466	79.28	61.29	48.10	38.31	30.85	25.09	20.67	17.34
	0.0712	70.13	54.62	43.08	34.62	28.15	23.11	19.29	16.26
	0.0970	62.91	49.68	39.69	32.06	26.28	21.77	18.25	15.47
	0.1238	59.06	47.06	37.87	30.85	25.35	21.12	17.78	15.16
	0.1518	51.79	41.82	34.01	27.93	23.12	19.40	16.44	14.09
	0.1810	50.09	40.69	33.29	27.56	22.98	19.33	16.43	14.08
ν/cS	0.0466	76.72	59.55	46.92	37.53	30.34	24.79	20.51	17.29
	0.0712	68.31	53.42	42.30	34.13	27.87	22.98	19.27	16.33
	0.0970	61.81	49.01	39.32	31.89	26.26	21.85	18.41	15.71
	0.1238	58.50	46.81	37.83	30.96	25.55	21.39	18.12	15.57
	0.1518	51.73	41.96	34.29	28.33	23.58	19.93	17.01	14.76
	0.1810	50.47	41.19	33.86	28.19	23.63	20.00	17.14	14.94
$c/\text{m} \cdot \text{s}^{-1}$	0.0466	1635.7	1620.4	1604.9	1589.3	1574.0	1558.4	1542.5	1526.6
	0.0712	1591.1	1576.0	1560.7	1545.7	1530.2	1514.6	1499.0	1483.1
	0.0970	1549.6	1534.8	1519.6	1504.3	1488.9	1473.2	1457.2	1441.4
	0.1238	1506.9	1491.9	1476.8	1461.6	1446.5	1431.1	1415.4	1399.6
	0.1518	1470.3	1455.4	1440.4	1425.2	1409.9	1394.8	1379.2	1363.5
	0.1810	1426.8	1411.9	1396.6	1381.4	1366.2	1350.8	1335.3	1319.6
nD	0.0466	1.436	1.433	1.429	1.428	1.427	1.427	–	–
	0.0712	1.429	1.428	1.426	1.424	1.423	1.422	–	–
	0.0970	1.425	1.424	1.425	1.420	1.419	1.418	–	–
	0.1238	1.421	1.419	1.418	1.416	1.416	1.413	–	–
	0.1518	1.415	1.414	1.412	1.411	1.411	1.411	–	–
	0.1810	1.412	1.409	1.408	1.408	1.407	1.406	–	–

^a The standard uncertainties u (0.68 level of confidence) are $u(T) = 0.01 \text{ K}$, $u(P) = 0.2 \text{ kPa}$, $u(\rho) = 0.50 \text{ kg} \cdot \text{m}^{-3}$, $u(\eta) = 0.07 \text{ mPa} \cdot \text{s}$, $u(\nu) = 0.09 \text{ cS}$, $u(nD) = 0.001$, $u(c) = 0.5 \text{ m} \cdot \text{s}^{-1}$, $u(x) = 0.0001$

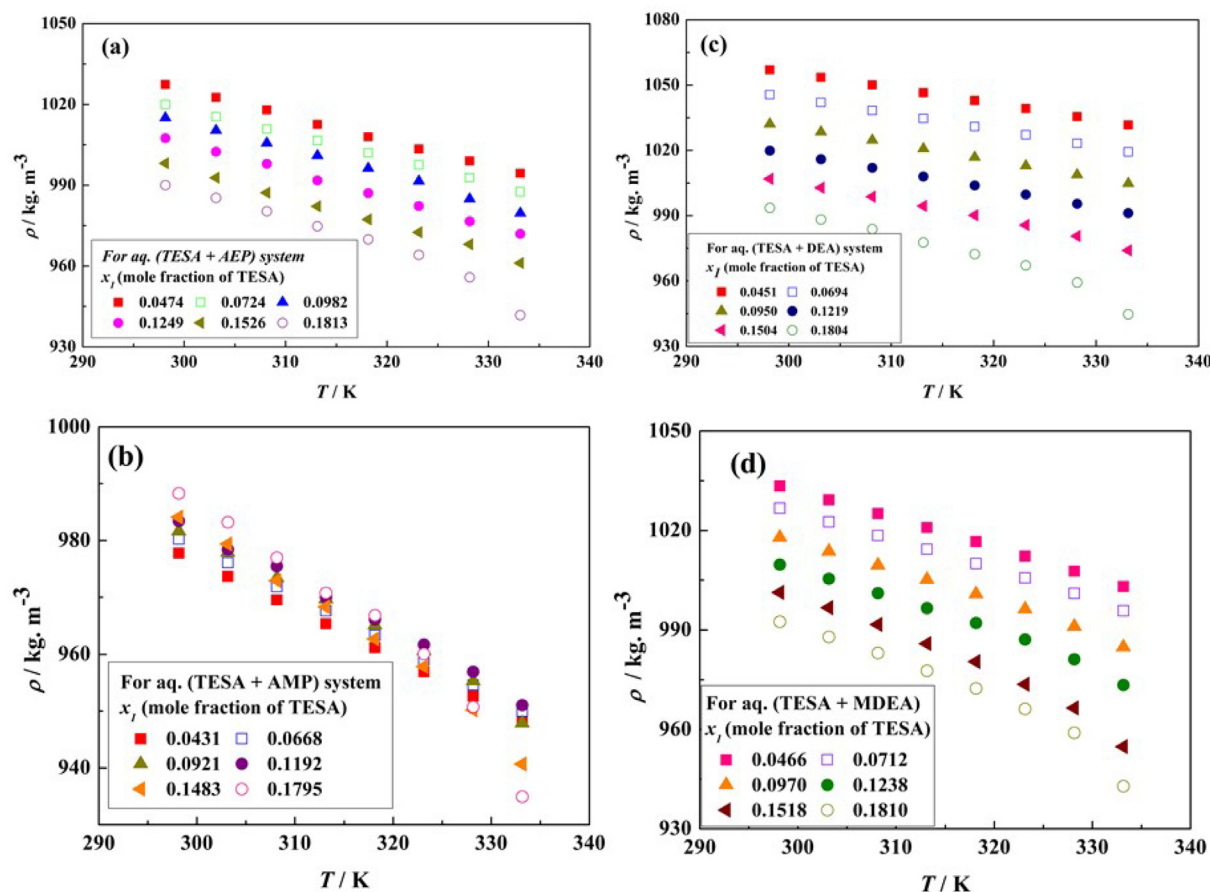


Fig. 1. Experimental densities of (a) aq. (TESA + AEP), (b) aq. (TESA + AMP), (c) aq. (TESA + DEA) and (d) aq. (TESA + MDEA) systems as a function of temperature at varied mole fractions of TESA.

contrast, aqueous (TESA+AMP) exhibits an opposite trend with TESA concentration. (Fig. 1 (b)).

Three models were applied in this work to explore the detailed relations of density with temperature and solvent compositions over the studied solvents: (i) Modified Redlich-Kister model, (ii) an empirical model M_I , and (iii) Neural network model.

3.1.1. Modified Redlich-Kister model

Prior research work has applied the Modified Redlich-Kister to correlate the density and excess molar volumes for binary and

ternary amine systems [25,26]. A similar theory was applied for aqueous TESA-amine mixtures in the present work. The model can be articulated as:

$$V_{jk}^E/m^3.kmol^{-1} = x_j x_k \sum_{p=0}^N A_p (x_j - x_k)^p \quad (1)$$

where A_p is the temperature-dependent parameter and N indicates the total number of such optimized pair parameters. The temperature dependency of the above-mentioned pair parameter can be represented as below:

Table 6

Binary parameters (A_0 , A_1 , and A_2) of Redlich-Kister model for the excess volume for (i) TESA (1) + AEP (2) + H₂O (3), (ii) TESA (1) + AMP (2) + H₂O (3), (iii) TESA (1) + DEA (2) + H₂O (3) & (iv) TESA (1) + MDEA (2) + H₂O (3).

Parameters	System	(i) TESA (1) + AEP (2) + H ₂ O (3)			(ii) TESA (1) + AMP (2) + H ₂ O (3)			(iii) TESA (1) + DEA (2) + H ₂ O (3)			(iv) TESA (1) + MDEA (2) + H ₂ O (3)		
		TESA + AEP	AEP + H ₂ O	TESA + H ₂ O	TESA + AMP	AMP + H ₂ O	TESA + H ₂ O	TESA + DEA	DEA + H ₂ O	TESA + H ₂ O	TESA + MDEA	MDEA + H ₂ O	TESA + H ₂ O
A_0	r	26.472	-5.915	-5.574	0.513	-2.469	1.136	4.959	-1.135	0.592	-0.625	1.605	1.647
	s	-0.169	0.039	0.038	-0.005	0.016	-0.006	-0.033	0.009	-0.002	0.005	-0.010	-0.010
	$t \times 10^5$	26.941	-6.301	-6.032	1.192	-2.413	1.022	5.329	-1.488	0.412	-1.006	1.841	1.747
A_1	r	23.221	-47.531	-4.847	19.064	-17.629	-0.944	1.653	-9.893	-1.010	-13.565	7.171	-0.082
	s	-0.161	0.308	0.031	-0.111	0.107	0.005	-0.014	0.067	0.006	0.099	-0.053	-0.001
	$t \times 10^5$	27.589	-49.854	-4.977	15.762	-16.107	-0.854	2.861	-11.259	-0.994	-17.708	9.771	0.175
A_2	r	-481.808	-75.313	13.463	-91.486	-25.432	0.744	-50.985	-17.879	1.212	79.592	6.722	-0.856
	s	3.164	0.488	-0.087	0.547	0.157	-0.004	0.349	0.119	-0.008	-0.590	-0.053	0.007
	$t \times 10^5$	-517.264	-78.841	14.055	-80.496	-23.914	0.675	-60.245	-19.992	1.285	107.728	10.020	-1.349
AAD(%)		0.044			0.087			0.041			0.070		
SD		0.711			1.180			0.732			0.993		

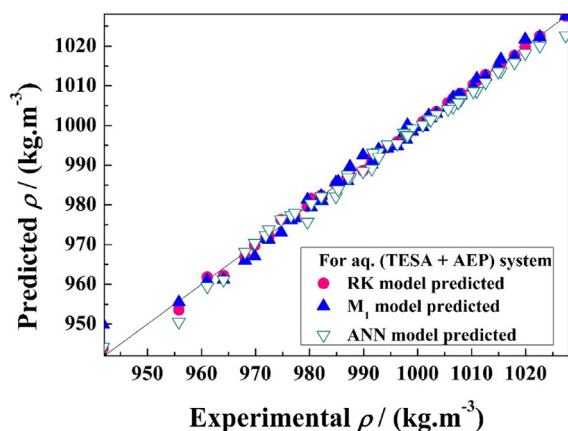


Fig. 2. Parity plot: Comparison of experimental and predicted density, $\rho/\text{kg.m}^{-3}$, for aq. (TESA + AEP) blend.

$$A_p = r + s(T/K) + t(T/K)^2 \quad (2)$$

Further, the excess volume for the ternary system:

$$V_E = V_{12}^E + V_{13}^E + V_{23}^E \quad (3)$$

The excess molar volumes were further estimated using the experimental density data of all TESA -amine mixtures using Eq. (4).

$$V_E = V_m - \sum x_i V_i^0 \quad (4)$$

where V_i^0 are the pure component molar volume and V_m molar volume of the TESA-amine blend at the system temperature. Additionally, the molar volume of the TESA-amine blends was estimated using the experimentally measured density as follows:

$$V_m = \frac{\sum x_i M_i}{\rho_m} \quad (5)$$

where M_i is the pure component molar mass of component i , ρ_m is experimentally measured liquid density, and x_i is mole fraction of the pure component i .

The temperature-dependent parameters in Eq. (1) for the aqueous ternary mixtures have been obtained by regression of experimental data within the temperature range of 298.15–333.15 K (Table 6). The average absolute deviation (AAD) amid the calculated and experimental results is determined by using Eq. (6).

$$\%AAD = \frac{100}{N} \times \sum_{i=1}^N \frac{|X_{\text{calculated},i} - X_{\text{experimental},i}|}{X_{\text{experimental},i}} \quad (6)$$

A low AAD value indicates a good agreement between the experimental results and the densities calculated from Eq1. The AAD is

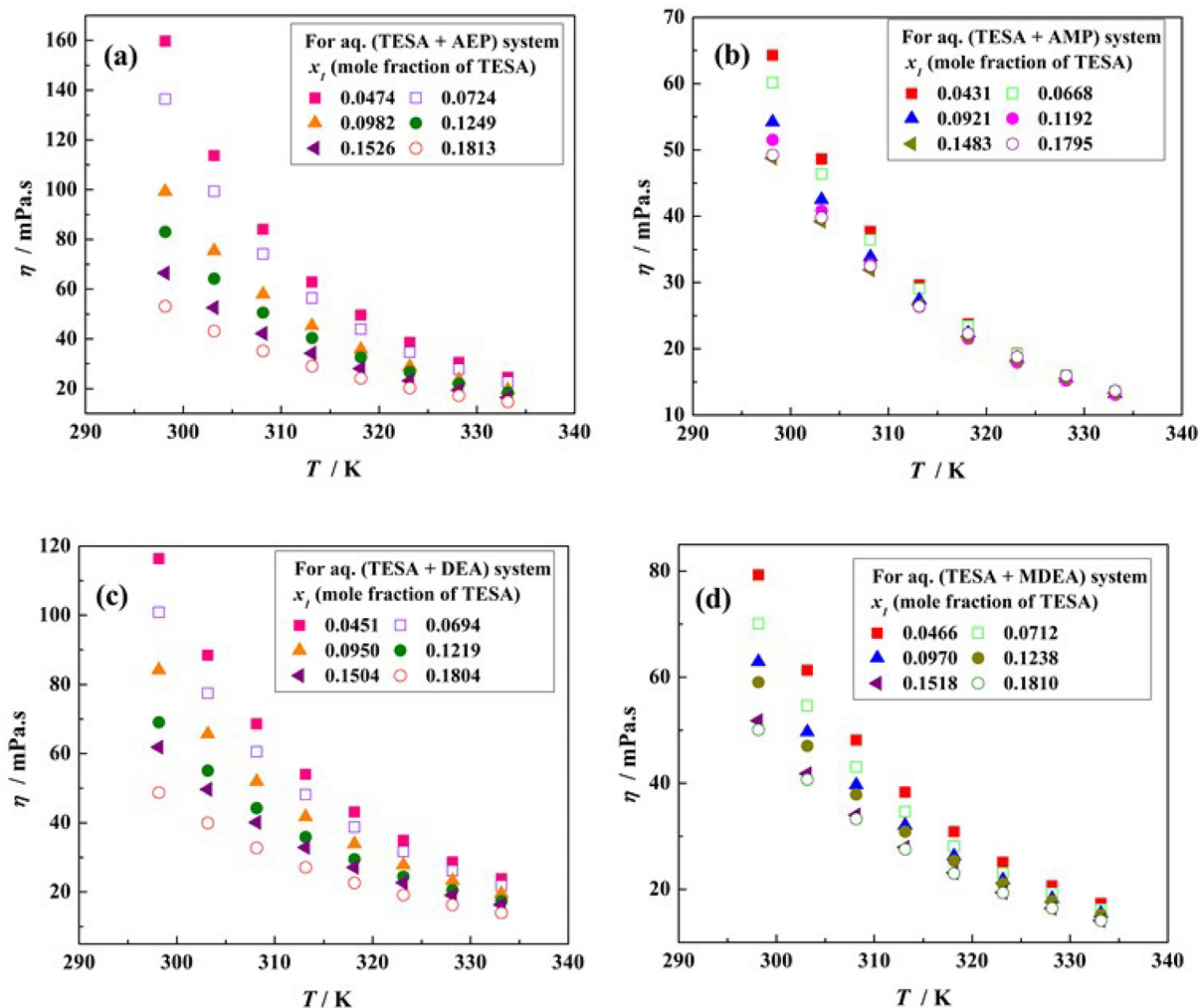
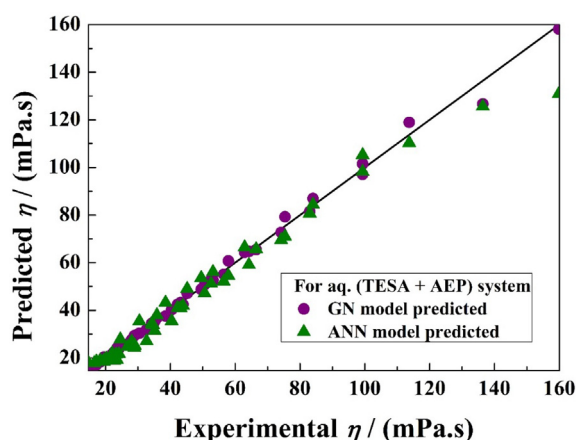


Fig. 3. Experimental viscosities of (a) aq. (TESA + AEP), (b) aq. (TESA + AMP), (c) aq. (TESA + DEA) and (d) aq. (TESA + MDEA) systems as a function of temperature at varying compositions.

Table 7Parameters of the Grunberg-Nissan model for (i) TESA (1) + AEP (2) + H₂O (3), (ii) TESA (1) + AMP (2) + H₂O (3), (iii) TESA (1) + DEA (2) + H₂O (3) & (iv) TESA (1) + MDEA (2) + H₂O (3).

Parameters	Blend	(i) TESA (1) + AEP (2) + H ₂ O (3)	(ii) TESA (1) + AMP (2) + H ₂ O (3)	(iii) TESA (1) + DEA (2) + H ₂ O (3)	(iv) TESA (1) + MDEA (2) + H ₂ O (3)
G_{12}	$r \times 10^{-2}$	-3.429	-12.582	-0.920	1.531
	s	2.024	7.846	0.560	-1.105
	$t \times 10^4$	-30.177	-122.466	-8.506	18.990
G_{23}	$r \times 10^{-2}$	2.629	2.196	1.134	0.959
	s	-1.367	-1.274	-0.574	-0.429
	$t \times 10^4$	18.877	19.278	7.982	5.366
G_{31}	$r \times 10^{-2}$	1.094	0.506	1.062	1.095
	s	-0.445	-0.062	-0.428	-0.440
	$t \times 10^4$	5.325	-0.905	5.055	5.162
	AAD(%)	1.992	2.315	1.590	1.210
	SD	2.022	1.878	0.802	0.529

**Fig. 4.** Parity plot: Comparison of experimental and predicted viscosity, $\eta/\text{mPa.s}$, for aq. (TESA + AEP) blend.

0.087% for (TESA + AMP), 0.044% for (TESA + AEP), 0.070% for (TESA + MDEA) and 0.041% for (TESA + DEA) systems, indicating that the modified Redlich – Kister predicts the density of the tested amine mixture well.

3.1.2. An empirical model M_1

In our previous work [24], the following regressive empirical model was found to be accurate for correlating sound velocity and refractive index. Therefore, for the present work also, along with sound velocity and refractive index, the same model is tested for correlation of density.

$$Y = A + (B \times x_1) + \left(\frac{C}{x_2}\right) + \left(\frac{D}{T}\right) + \left(E \times \frac{x_1}{x_2}\right) + \left(F \times \frac{x_1}{T}\right) + \left(\frac{G}{T \times x_2}\right) + \left(\frac{H \times x_1}{T \times x_2}\right) \quad (7)$$

where, Y could be density (ρ) in kg.m^{-3} or refractive index (n_D) or sound velocity (c) in m.s^{-1} ; x_1 is the mass fraction of AMP, AEP, MDEA, or DEA; and x_2 is the mass fraction of TESA and A, B, C, D, E, F, G , and H are regressed constants for the blends under study. As the mass fraction of water is constant in all the compositions, it is not considered to be a variable in Eq. (7). The AAD and standard deviations for the density of aqueous ternary mixtures of (TESA + AEP) (TESA + AMP), (TESA + DEA) and (TESA + MDEA) using model M_1 have been calculated and presented in Table S1. The AAD using the model M_1 for densities of (TESA + AEP), (TESA + AMP), (TESA + DEA) and (TESA + MDEA) systems are found to be 0.115, 0.159, 0.125 and 0.151%, respectively. The values of AAD found using Eq. (7) are reasonably low in comparison to the Redlich-Kister equation which makes it a good statistical model for the prediction of similar properties.

3.1.3. Neural network model

Artificial neural networks are very successful in correlating various complex and non-linear functions in the literature, particularly for the CO₂ capture process [27], vapor-liquid-solid equilibrium [28], thermophysical or thermodynamic properties, etc. [29–31]. Hence, the thermophysical properties were attempted to be correlated by using ANN techniques. We applied an ANN model with a multilayer feed-forward ANN with a back-propagation algorithm using the Levenberg-Marquardt back-propagation method as a training function, log sigmoid and linear as the transfer functions for hidden and output layers along with the normalization of the initial data to build the relations between density, viscosity, sound velocity, and refractive index. The number of neurons was taken to be 13 for the present work very near to our previous work [24]. The AAD, standard deviations and mean squared error (MSE) of density for the ternary aqueous mixture of (TESA + AMP), (TESA + AEP), (TESA + MDEA), and (TESA + DEA) using ANN have been calculated and presented in Table S2. The AAD using the ANN for densities of (TESA + AMP), (TESA + AEP), (TESA + MDEA) and (TESA + DEA) systems are found to be 0.087, 0.140, 0.228 and 0.061%, respectively. The predictions from the Redlich-Kister equation is more accurate in comparison to the ANN and model M_1 . A parity comparison of experimental and predicted density using the Redlich-Kister model, ANN, and model M_1 for the aqueous (TESA + AEP), (Fig. 2) indicates that all three models do fit well with the experimental data.

The behavior of excess molar volumes for the aqueous systems of (TESA + AEP), (TESA + AMP), (TESA + DEA), and (TESA + MDEA) are represented in Table S3. Excess molar volumes were found to increase with temperature and the composition of TESA for all the blends. The positive values of excess molar volume over the tested temperature range and compositions indicate the presence of physical interactions such as dispersion forces in the blends. Moreover, the negative contributions can be encountered due to various chemical interactions such as charge-transfer-type forces, hydrogen bond formation/breakage, and other complex interactions like donor-acceptor, dipole-dipole, and dipole induced dipole. The experimental density values for the (TESA + AEP), (TESA + AMP), (TESA + DEA) and (TESA + MDEA) aqueous ternary mixtures are used to calculate the density deviations ($\Delta\rho$), which is represented by the following Eq. (8):

$$\Delta\rho = \rho_{\text{exp}} - (x_1 \times \rho_1 + x_2 \times \rho_2 + x_3 \times \rho_3) \quad (8)$$

where, ρ_{exp} is the experimental density of mixtures, x_1, x_2, x_3 represent the mole fractions, and ρ_1, ρ_2, ρ_3 the densities of pure TESA, water, and AMP/AEP/MDEA/DEA, respectively. The density deviations for (TESA + AMP), (TESA + AEP), (TESA + MDEA) and (TESA + DEA) aqueous mixtures are represented in Table S4. It is clear from the results that densities of the four mixtures show a negative deviation from ideality at high temperature (majorly from 308.15 to 333.15 K) and concentration of TESA. Whereas the values at low temperatures and compositions of TESA are positive except for the ternary aqueous mixture of (TESA +

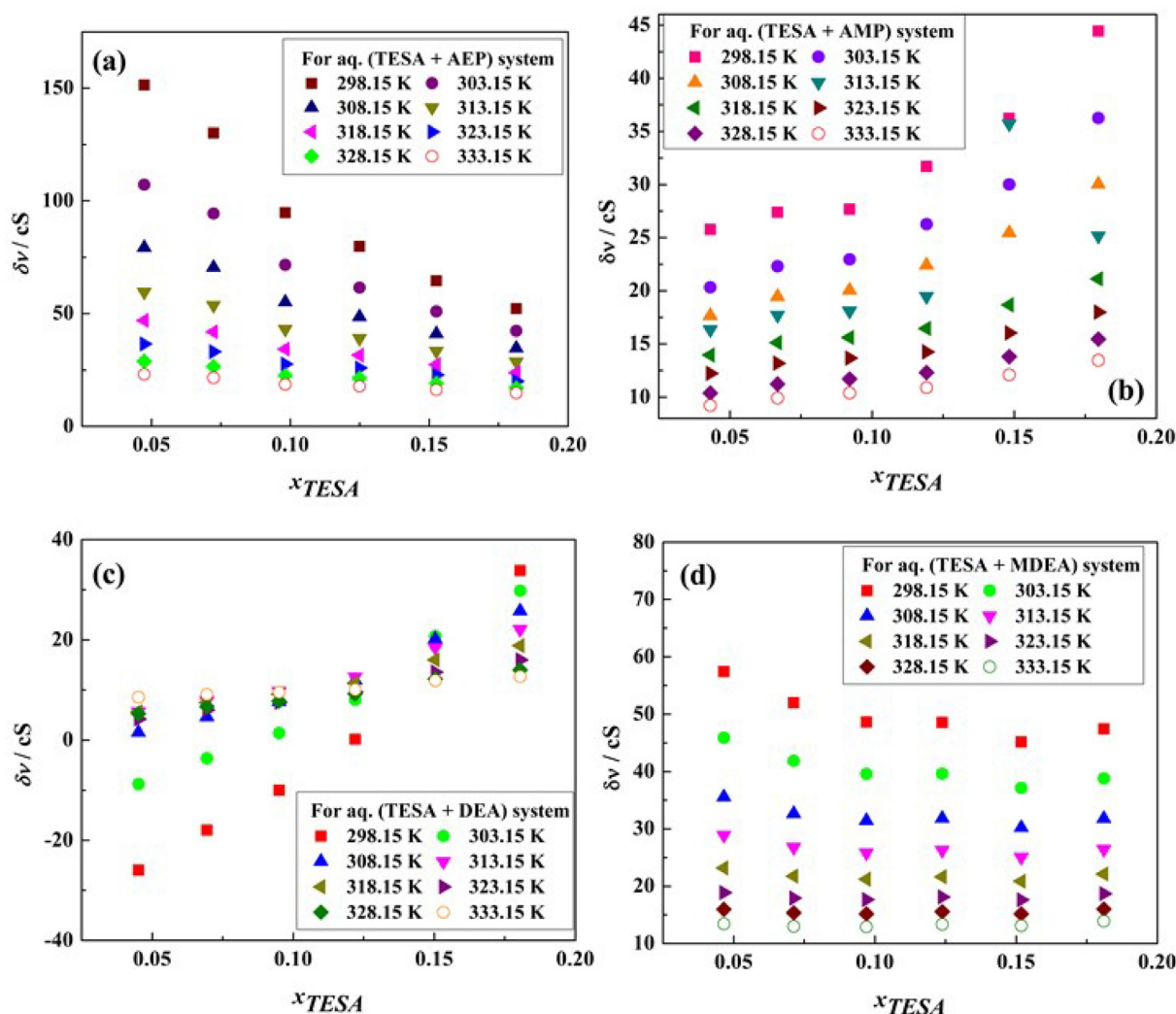


Fig. 5. Viscosities deviations, δv / cS, of (a) aq. (TESA + AEP), (b) aq. (TESA + AMP), (c) aq. (TESA + DEA) and (d) aq. (TESA + MDEA) as function of temperature and composition of the blends.

AMP). For the ternary aqueous mixture of (TESA + AMP), all the values are negative.

Further, the thermal expansion of the blends at the atmospheric pressure as a function of temperature is calculated using the thermal expansion coefficient using the experimentally measured density as:

$$\alpha = -\frac{1}{\rho_m} \left(\frac{\partial \rho_m}{\partial T} \right)_P \quad (9)$$

where α is the thermal expansion coefficient and ρ_m is the experimentally measured density at a specific pressure (P) and temperature (T). The values of the thermal expansion coefficient are important for the designing of the carbon capture and sequestration (CCS) system. The attribution of the variable yields the correlation of volume expansion of the solvent blends as a function of temperature and pressure. The values of thermal expansion coefficients of all the four blends were found to increase with TESA concentration and temperatures. The details can be found in Table S5.

3.2. Viscosity

The costs of solvent circulation and mixing for enhanced CO_2 capture capacity is related to the transport properties such as viscosity and

diffusivity. The high viscosity of the solvent slows down the diffusion process that thus degrades the CO_2 absorption rate and also causes significantly high pumping costs. Both make the overall process energy-intensive. The viscosity is a reflection of the intermolecular interactions. The viscosities of both the ternary aqueous mixtures of (TESA + AEP), (TESA + AMP), (TESA + DEA), and (TESA + MDEA) decrease with temperature and the concentration of TESA (Tables (2–5) and Fig. 3). We also observed that the aqueous (TESA + AMP) varied less significantly with temperatures and TESA concentrations than the other three blends.

The viscosity data of the present work are correlated using: (i) Grunberg and Nissan Model and (ii) Neural network model.

Conventionally, the Grunberg & Nissan Model is found to be precise and efficient to correlate experimental viscosity of the ternary liquid systems [12,26]. The Grunberg & Nissan model is given by:

$$\ln \eta_m / \text{mPa.s} = \sum x_i \ln \eta_i + \sum \sum x_i x_j G_{ij} \quad (10)$$

where η_i is the dynamic viscosity of the pure constituent and x_i the mole fraction of the i th constituent in the solution. For a ternary system, the equation can be given as:

$$\ln \eta_m = (x_1 \times \ln \eta_1) + (x_2 \times \ln \eta_2) + (x_3 \times \ln \eta_3) + (x_1 \times x_2 \times G_{12}) + (x_1 \times x_3 \times G_{13}) + (x_2 \times x_3 \times G_{23}) \quad (11)$$

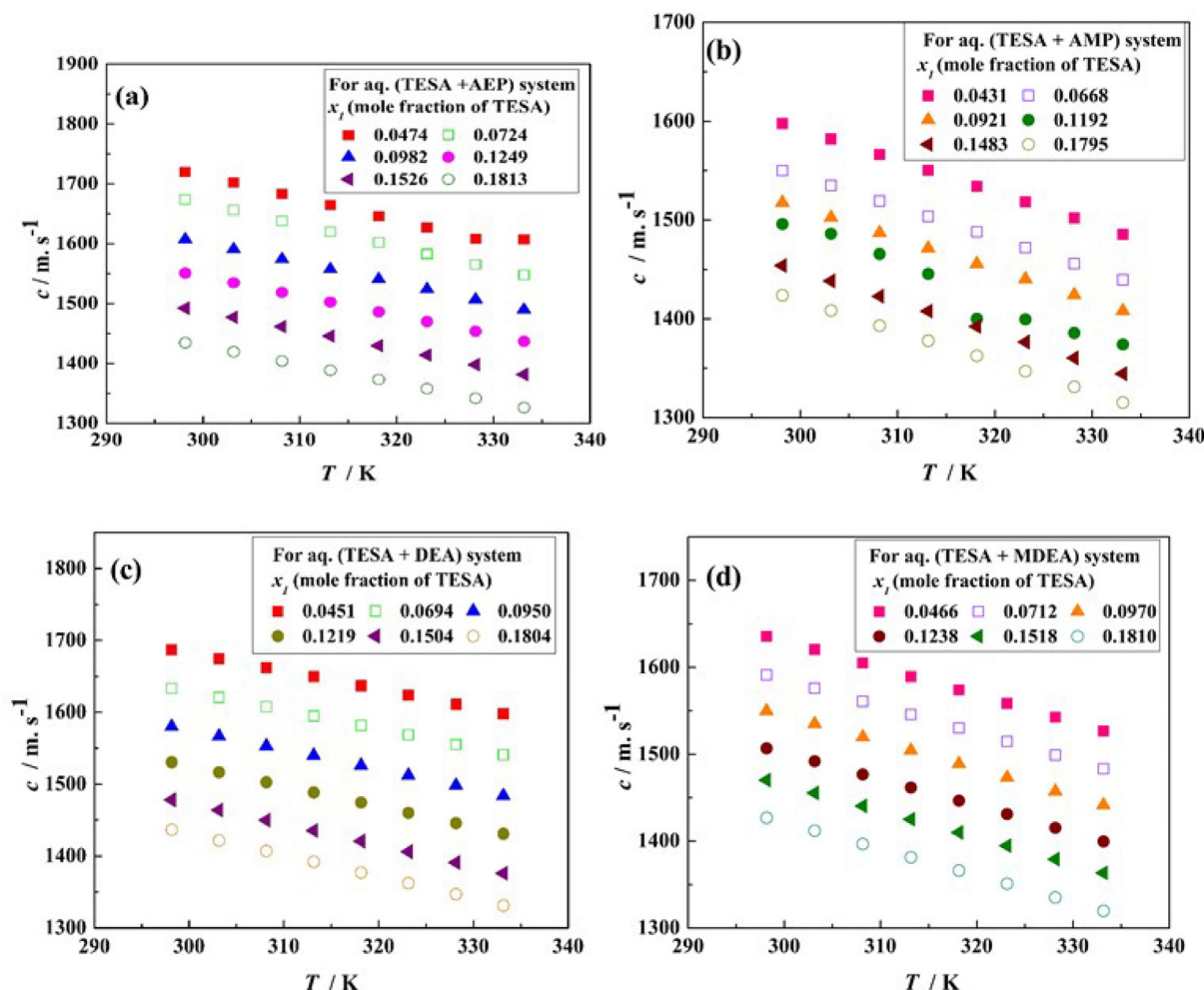


Fig. 6. Experimental sound velocity, $c/\text{m.s}^{-1}$, of (a) aq. (TESA + AEP), (b) aq. (TESA + AMP), (c) aq. (TESA + DEA) and (d) aq. (TESA + MDEA) as function of temperature and composition of the blends.

where G_{ij} are temperature reliant factors estimated from Eq. (12).

$$G_{ij} = r + s(T/K) + t(T/K)^2 \quad (12)$$

The regressed temperature-dependent parameters of Eq. (12) are reported in Table 7. The AAD between the experimental and modeled data for the (TESA + AEP), (TESA + AMP), (TESA + DEA) & (TESA + MDEA) aqueous systems is found to be 1.992, 2.315, 1.590, and 1.210, respectively. As expected, the Grunberg and Nissan's model fits well overall the aqueous systems studied in this work. The AAD using the ANN for dynamic viscosities of aqueous (TESA + AEP), (TESA + AMP), (TESA + DEA), and (TESA + MDEA) systems are found to be 7.705, 2.502, 0.040, and 1.783%, respectively. The predictions from the ANN model are found to be comparable to the Grunberg & Nissan Model. The AAD, standard deviations, and MSE of dynamic viscosity for the aqueous ternary mixture of (TESA + AEP), (TESA + AMP), (TESA + DEA), and (TESA + MDEA) using ANN have been calculated and presented in Table S2. As indicated in Fig. 4 for the aqueous ternary system of (TESA + AEP) both the first principle Grunberg & Nissan Model and the ANN provide a good prediction of viscosities of the studied blends.

The kinematic viscosity deviations (Δv) from ideality were calculated using the values of experimental viscosity for the ternary aqueous mixtures of (TESA + AEP), (TESA + AMP), (TESA + DEA), and (TESA + MDEA) according to:

$$\Delta v = v_{\text{exp}} - (x_1 \times v_1 + x_2 \times v_2 + x_3 \times v_3) \quad (13)$$

where v is the kinematic viscosity of blends; x_1 , x_2 , and x_3 are the mole fractions; v_1 , v_2 , and v_3 are the kinematic viscosities; the subscripts 1, 2, and 3 represent pure TESA, water, and pure AMP/AEP/MDEA/DEA.

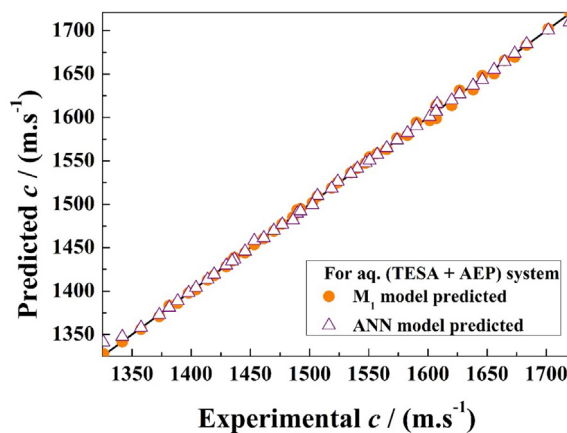


Fig. 7. Parity plot: Comparison of experimental and predicted sound velocity, $c/\text{m.s}^{-1}$, for aq. (TESA + AEP).

Table 8

Isentropic compressibility, $K_s \times 10^{10}$, m.s.kg^{-1} for (i) TESA (1) + AEP (2) + H₂O (3), (ii) TESA (1) + AMP (2) + H₂O (3), (iii) TESA (1) + DEA (2) + H₂O (3) and (iv) TESA (1) + MDEA (2) + H₂O (3) from (298.15–333.15) K.

T/K	298.15	303.15	308.15	313.15	318.15	323.15	328.15	333.15
x_1	TESA (1) + AEP (2) + H ₂ O (3)							
0.0474	3.291	3.377	3.467	3.564	3.662	3.766	3.873	3.894
0.0724	3.501	3.592	3.686	3.785	3.891	4.009	4.112	4.229
0.0982	3.816	3.913	4.014	4.120	4.231	4.344	4.473	4.601
0.1249	4.128	4.235	4.345	4.467	4.588	4.712	4.848	4.986
0.1526	4.499	4.618	4.744	4.873	5.007	5.144	5.288	5.453
0.1813	4.909	5.038	5.175	5.321	5.469	5.628	5.811	6.041
x_1	TESA (1) + AMP (2) + H ₂ O (3)							
0.0431	4.007	4.104	4.205	4.310	4.420	4.533	4.653	4.779
0.0668	4.245	4.348	4.458	4.572	4.688	4.813	4.943	5.081
0.0921	4.423	4.531	4.647	4.763	4.890	5.019	5.162	5.323
0.1192	4.544	4.629	4.772	4.933	5.281	5.309	5.443	5.568
0.1483	4.808	4.935	5.076	5.211	5.359	5.511	5.687	5.882
0.1795	4.993	5.127	5.274	5.427	5.571	5.741	5.936	6.183
x_1	TESA (1) + DEA (2) + H ₂ O (3)							
0.0451	3.324	3.385	3.448	3.511	3.578	3.648	3.721	3.797
0.0694	3.585	3.654	3.726	3.800	3.877	3.958	4.043	4.132
0.0950	3.881	3.962	4.046	4.132	4.223	4.318	4.416	4.519
0.1219	4.185	4.279	4.376	4.477	4.582	4.691	4.806	4.927
0.1504	4.544	4.652	4.763	4.881	5.003	5.132	5.269	5.422
0.1804	4.875	5.006	5.134	5.276	5.422	5.573	5.747	5.973
x_1	TESA (1) + MDEA (2) + H ₂ O (3)							
0.0466	3.617	3.700	3.788	3.878	3.970	4.068	4.171	4.278
0.0712	3.847	3.937	4.031	4.127	4.228	4.335	4.446	4.566
0.0970	4.091	4.188	4.289	4.396	4.507	4.625	4.752	4.887
0.1238	4.362	4.469	4.580	4.698	4.817	4.946	5.087	5.244
0.1518	4.620	4.737	4.861	4.994	5.131	5.279	5.439	5.633
0.1810	4.949	5.078	5.215	5.360	5.509	5.672	5.848	6.091

Further, the deviations of viscosity from ideality originate from the varied properties of the blend compositions such as molecular size, conformation, dipole moments, and polarities. The values of viscosity deviations for (TESA + AEP), (TESA + AMP), (TESA + DEA), and (TESA + MDEA) aqueous mixtures are represented in Table S6 and Fig. 5. We noted from Fig. 5(b) that for the (TESA + AMP) blends, a maximum deviation of 44.446 cS occurs at $x_{\text{TESA}} = 0.17$ and at 298.15 K. The deviations of (TESA + AMP) are positive across the tested conditions and tend to become low at elevated temperatures and reduced TESA level. A positive value of deviation indicates a strong intermolecular interaction in the blends. For the aqueous ternary systems (TESA + AEP) and (TESA + MDEA), in contrast, we observed a drop in the kinematic viscosity deviations with increasing temperature and TESA concentration. The viscosity deviations for the ternary aqueous mixture of (TESA + DEA) become negative at temperatures below 303.15 K and $x_{\text{TESA}} < 0.095$. Additionally, the viscosity deviations are found to be more significant and more temperature-dependent than the deviations of density and refractive index data.

3.3. Sound velocity

CO₂ capture is a pressure-driven process, and the speed of sound is hence one of the important properties to measure. From the experimental values obtained, we observed that the sound velocities become slow for all the ternary aqueous blends of (TESA + AEP), (TESA + AMP), (TESA + DEA), and (TESA + MDEA) at higher temperatures and increase in TESA concentration (Tables 2–5) & Fig. 6). The effect on sound velocity from temperature can be explained by the accelerated molecular motion amid the blends at elevated temperatures.

Two models served to correlate the experimental data: (1) model M_1 and (2) Artificial neural network model, which have been described in Section 3.1. The AAD and standard deviations of sound velocity for the

four blends using model M_1 are presented in Table S7. The AAD using the model M_1 for sound velocities in (TESA + AEP), (TESA + AMP), (TESA + DEA) and (TESA + MDEA) aqueous systems are found to be 0.150, 0.208, 0.134, and 0.103%, respectively. The AAD, standard deviations, and MSE of sound velocity for the blends using ANN are presented in Table S2.

The AAD using the ANN for sound velocities in aqueous ternary mixtures of (TESA + AEP), (TESA + AMP), (TESA + DEA) and (TESA + MDEA) are found to be 0.101, 0.374, 0.116, and 0.103%, respectively. The comparison of both the models for the aqueous ternary mixture of (TESA + AEP), as shown in Figs. 7, demonstrates the competency of model M_1 and ANN model to predict the velocity of sound.

Another important temperature-dependent acoustic property (viz. isentropic compressibility) can be estimated using Eq. (14) (Table 8).

$$K_s = \frac{1}{\rho \times c^2} \quad (14)$$

where, $K_s/\text{m.s.kg}^{-1}$ is the isentropic compressibility, $c/\text{m.s}^{-1}$ is the experimental sound velocity and $\rho/\text{kg.m}^{-3}$ is the experimental density of the ternary aqueous blends at varying temperatures and compositions of TESA.

3.4. Refractive index

The tested refractive indices (n_D) of (TESA + AEP), (TESA + AMP), (TESA + DEA), and (TESA + MDEA) blends generally decrease with temperature up to 323.15 K and TESA concentration (Tables 2–5 & Fig. 8). The dependency of n_D on temperature can be explained by the weakened forces of molecular attractions which lead to an intensified collision between stray light and blend molecules. When the temperature is higher than 323.15 K, it is extremely challenging to measure the n_D values of the blends repeatably. This could be associated with the structural changes in the blends at >323.15 K.

The experimental refractive index data can also be described by the empirical model M_1 and ANN model. The AAD and standard deviations of the refractive index for the aqueous ternary mixtures using model M_1 have been calculated and presented in Table S8. The AAD of using the model M_1 to predict refractive indices of (TESA + AEP), (TESA + AMP), (TESA + DEA) and (TESA + MDEA) aqueous systems are 0.038, 0.045, 0.046, and 0.048%, respectively. The AAD of applying ANN for (TESA + AEP), (TESA + AMP), (TESA + DEA) and (TESA + MDEA) are 0.057, 0.075, 0.028, and 0.064%, respectively. The AAD, standard deviations, and MSE of the refractive index for the blends using ANN were calculated and summarized in Table S2. The comparison of both the models shown in Fig. 9 for the (TESA + AEP) demonstrates that the ANN model predicts the data more accurately than the model M_1 .

3.5. Diffusivity of CO₂

The kinetics of CO₂ the capture solvent depends on the mass transfer rate, which is a function of physical solubility and diffusivity of CO₂ along with density and viscosity. Due to the similarities in the electronic structure and molecular volume, N₂O is commonly used as a non-reacting gas to predict the diffusivity of CO₂ [32]. Also, the solubility of N₂O in solvents can be predicted by empirical relations developed by Versteeg and Swaaij [32]. The CO₂ diffusivity can be estimated by making an analogy to the N₂O. The N₂O diffusivity in (TESA + amine) blends was calculated as a function of the dynamic viscosity (η) according to the modified Stokes-Einstein correlation:

$$(D_{\text{N}_2\text{O}} \times \eta^{0.8})_{\text{TESA+AMINE}} = \text{constant} = (D_{\text{N}_2\text{O}} \times \eta^{0.8})_{\text{water}} \quad (15)$$

The relations of diffusivity between CO₂ and N₂O in water as proposed by Versteeg and van Swaaij [31] are given by:

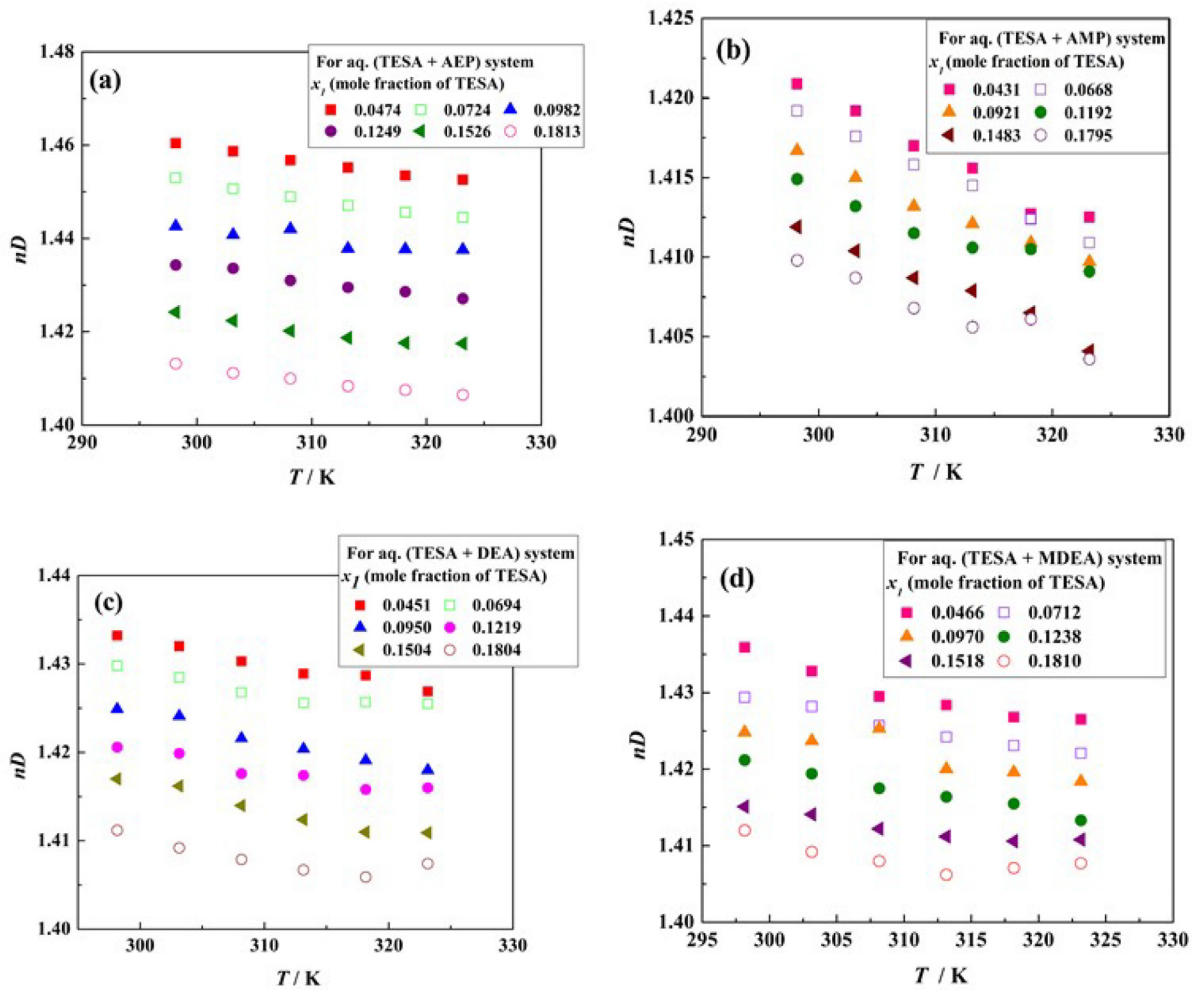


Fig. 8. Experimental refractive index, nD , of (a) aq. (TESA + AEP), (b) aq. (TESA + AMP), (c) aq. (TESA + DEA) and (d) aq. (TESA + MDEA) as function of temperature and composition of the blends.

$$D_{N_2O} = 5.07 \times 10^{-6} \times \exp\left(-\frac{2371}{T}\right) \quad (16)$$

$$D_{CO_2} = 2.35 \times 10^{-6} \times \exp\left(-\frac{2119}{T}\right) \quad (17)$$

We calculated the CO_2 diffusivity in the (TESA + amine) blends by using Eq. (18):

$$(D_{CO_2})_{TESA+AMINE} = (D_{N_2O})_{TESA+AMINE} \times \left(\frac{D_{CO_2}}{D_{N_2O}}\right)_{water} \quad (18)$$

where, $(D_{CO_2})_{TESA+AMINE}$ and $(D_{N_2O})_{TESA+AMINE}$ in $m^2.s^{-1}$ are the diffusivity of CO_2 and N_2O in the aq. (TESA + amine) blend at temperature T (K). The results as shown in Table S9 & Fig. 10 reveal that estimated diffusivities of CO_2 increase with temperatures and TESA concentrations in the tested blends, which could benefit the overall capture processes.

3.6. Thermodynamic properties

The thermodynamic properties of activation of viscous flow of the ternary mixtures (i.e., enthalpy of activation (ΔH), the entropy of activation (ΔS), and Gibbs energies of activation (ΔG)) were evaluated using Eyring's modified equation from Andrade's theory [33]. The kinematic viscosity can be derived from:

$$v = \frac{hN_A}{M} \exp\left(\frac{\Delta G}{RT}\right) \quad (19)$$

where, $M = \sum(x_i M_i)$ is the average molecular mass, h is Planck's constant (6.626×10^{-34} J.s), N_A is the Avogadro number (6.023×10^{23}

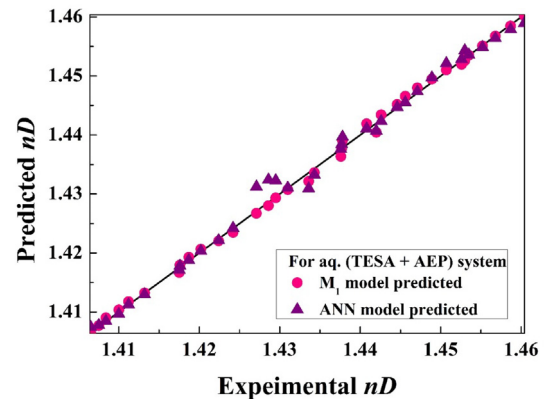


Fig. 9. Parity plot: Comparison of experimental and predicted refractive index, nD , for aq. (TESA + AEP).

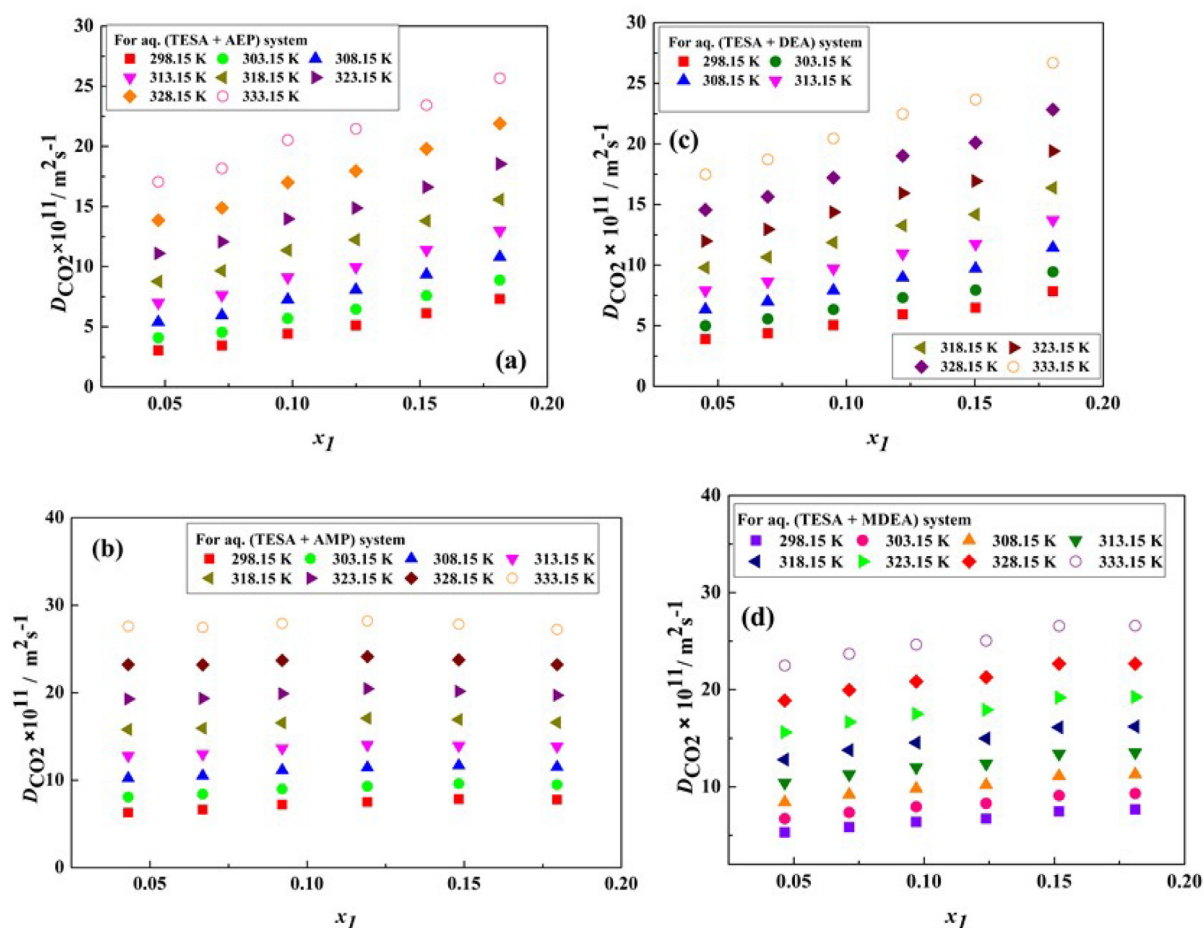


Fig. 10. Experimental sound velocity, $c/m.s^{-1}$, of (a) aq. (TESA + AEP), (b) aq. (TESA + AMP), (c) aq. (TESA + DEA) and (d) aq. (TESA + MDEA) as function of temperature and composition of the blends.

mol^{-1}), R is the universal gas constant ($8.314 J.mol^{-1} K^{-1}$), and T is the absolute temperature.

The ΔG values were estimated using equation 19 and were listed in Table 9. The ΔG values are positive for aqueous ternary systems of (TESA + AEP), (TESA + AMP), (TESA + DEA), and (TESA + MDEA) reflects strong intermolecular interactions between the components. These intermolecular interactions may be either physical or chemical depending on the orientation of bond length, bond angle, or subsequent interactions associated with the polar or nonpolar nature of the molecules.

Thermodynamically, the Gibbs free energy is characterized by:

$$\Delta G = \Delta H - T \times \Delta S \quad (20)$$

We calculated the changes of the entropy (ΔS) and enthalpy (ΔH) of activations by linear regression of the model as described by Eq. (20). Table 10 summarizes the data for the blend systems. The negative values of ΔS highlight the dependency of all the four systems on the transport properties especially the viscosity. The positive values of ΔH can again confirm the strong interactions among the components in each aqueous ternary system.

4. Conclusions

We measured new data of densities, viscosities, sound velocities, and refractive indices of aqueous (TESA + AEP), (TESA + AMP), (TESA + DEA), and (TESA + MDEA) systems over the temperature

range (298.15 to 333.15) K at varying compositions of the blends for CO_2 capture. The measured properties exhibit a direct correlation with temperature and compositions. Density, viscosity, sound velocity, and refractive index of all the blends show a decreasing trend with the increase in temperature and TESA concentration. This decreasing trend in the physical properties data is related to the weakened intramolecular interactions at elevated temperatures. Additionally, all the blends show positive values of excess molar volumes of the blends, which is likely due to their weak dispersion force. We found that all the first principle models and artificial neural network models can well describe the physicochemical properties of the blends. The data and the related models reported in our work provide opportunities for detailed kinetic studies of the CO_2 adsorption and feasibility evaluation to implement novel solvents in practical CO_2 capture processes.

Authors credit to work

Sweta Balchandani: Conceptualization, Data Curation, Formal analysis, Investigation, Software, Writing - original draft; Bishnupada Mandal: Conceptualization, Project administration, Supervision, Writing - review & editing; Sahil Garg: Conceptualization, Project administration, Supervision, Visualization, Writing - original draft preparation; Mengran Li: Conceptualization, Writing - review & editing; Swapnil Dharaskar: Data curation, Investigation, Writing - review & editing.

Table 9

Gibbs energies of activation of viscous flow, $\Delta G/\text{kJ mol}^{-1}$ for the viscous flow about (i) TESA (1) + AEP (2) + H₂O (3), (ii) TESA (1) + AMP (2) + H₂O (3), (iii) TESA (1) + DEA (2) + H₂O (3) and (iv) TESA (1) + MDEA (2) + H₂O (3) from (298.15–333.15) K.

T/K	298.15	303.15	308.15	313.15	318.15	323.15	328.15	333.15
x_i	TESA (1) + AEP (2) + H ₂ O (3)							
0.0474	58.852	58.993	59.202	59.423	59.752	60.025	60.327	60.660
0.0724	58.520	58.713	58.945	59.201	59.494	59.807	60.145	60.507
0.0982	57.788	58.074	58.367	58.682	59.018	59.377	59.759	60.156
0.1249	57.406	57.735	58.087	58.461	58.842	59.237	59.646	60.070
0.1526	56.923	57.299	57.697	58.101	58.516	58.942	59.385	59.847
0.1813	56.434	56.867	57.293	57.740	58.185	58.645	59.127	59.639
x_i	TESA (1) + AMP (2) + H ₂ O (3)							
0.0431	56.479	56.735	57.026	57.340	57.679	58.040	58.435	58.859
0.0668	56.389	56.692	57.019	57.364	57.728	58.109	58.521	58.961
0.0921	56.211	56.551	56.913	57.289	57.686	58.101	58.537	59.005
0.1192	56.167	56.536	56.912	57.286	57.673	58.099	58.564	59.057
0.1483	56.117	56.523	56.943	58.442	57.809	58.257	58.734	59.236
0.1795	56.225	56.642	57.074	57.514	57.957	58.425	58.914	59.429
x_i	TESA (1) + DEA (2) + H ₂ O (3)							
0.0451	57.871	58.158	58.474	58.809	59.166	59.537	59.923	60.332
0.0694	57.605	57.915	58.249	58.609	58.980	59.375	59.781	60.199
0.0950	57.254	57.598	57.957	58.336	58.729	59.133	59.562	60.005
0.1219	56.858	57.252	57.649	58.050	58.466	58.895	59.333	59.789
0.1504	56.687	57.095	57.502	57.926	58.354	58.802	59.255	59.737
0.1804	56.196	56.652	57.089	57.543	58.001	58.468	58.959	59.482
x_i	TESA (1) + MDEA (2) + H ₂ O (3)							
0.0466	57.054	57.372	57.708	58.063	58.428	58.803	59.196	59.624
0.0712	56.815	57.148	57.493	57.867	58.255	58.653	59.079	59.521
0.0970	56.619	56.984	57.359	57.745	58.153	58.573	59.012	59.472
0.1238	56.535	56.921	57.314	57.722	58.136	58.573	59.026	59.505
0.1518	56.283	56.699	57.118	57.547	57.981	58.439	58.912	59.418
0.1810	56.276	56.708	57.141	57.591	58.044	58.508	58.992	59.509

Table 10

Enthalpy of activation, $\Delta H/\text{kJ mol}^{-1}$, and entropy of activation, $\Delta S/\text{J K}^{-1} \text{mol}^{-1}$, for the viscous flow about (i) TESA (1) + AEP (2) + H₂O (3), (ii) TESA (1) + AMP (2) + H₂O (3), (iii) TESA (1) + DEA (2) + H₂O (3) and (iv) TESA (1) + MDEA (2) + H₂O (3).

x_i	$\Delta S/\text{J K}^{-1} \text{mol}^{-1}$	$\Delta H/\text{kJ mol}^{-1}$
x_i	TESA (1) + AEP (2) + H ₂ O (3)	
0.0474	−52.318	43.139
0.0724	−56.666	41.529
0.0982	−67.289	37.663
0.1249	−76.091	34.667
0.1526	−83.296	32.046
0.1813	−90.873	29.307
x_i	TESA (1) + AMP (2) + H ₂ O (3)	
0.0431	−67.639	36.224
0.0668	−73.015	34.551
0.0921	−79.384	32.479
0.1192	−81.430	31.833
0.1483	−86.807	30.357
0.1795	−90.971	29.057
x_i	TESA (1) + DEA (2) + H ₂ O (3)	
0.0451	−70.207	36.873
0.0694	−74.151	35.433
0.0950	−78.354	33.839
0.1219	−83.369	31.971
0.1504	−86.699	30.803
0.1804	−93.019	28.437
x_i	TESA (1) + MDEA (2) + H ₂ O (3)	
0.0466	−73.043	35.225
0.0712	−77.064	33.779
0.0970	−81.137	32.379
0.1238	−84.355	31.339
0.1518	−88.868	29.749
0.1810	−91.755	28.884

Notes

The authors declare no competing financial interest.

Declaration of Competing Interest

The authors declare that they have no known competing financial interests or personal relationships that could have appeared to influence the work reported in this paper.

Appendix A. Supplementary data

Supplementary data to this article can be found online at <https://doi.org/10.1016/j.molliq.2021.115440>.

References

- [1] B. Sreenivasulu, D. Gayatri, I. Sreedhar, K. Raghavan, A journey into the process and engineering aspects of carbon capture technologies, *Renew. Sust. Energ. Rev.* 41 (2015) 1324–1350.
- [2] S. Garg, G. Murshid, F.S. Mjalli, A. Ali, W. Ahmad, Experimental and correlation study of selected physical properties of aqueous blends of potassium sarcosinate and 2-piperidineethanol as a solvent for CO₂ capture, *Chem. Eng. Res. Des.* 118 (2017) 121–130.
- [3] P.T. Anastas, J.C. Warner, *Principles of green chemistry*, *Green Chem. Theor. Pract.* (1998) 29–56.
- [4] A. Haghtalab, A. Shojaeian, High pressure measurement and thermodynamic modeling of the solubility of carbon dioxide in N-methyldiethanolamine and 1-butyl-3-methylimidazolium acetate mixture, *J. Chem. Thermodyn.* 81 (2015) 237–244.
- [5] J. Aboudi, M. Vafaezadeh, Efficient and reversible CO₂ capture by amine functionalized-silica gel confined task-specific ionic liquid system, *J. Adv. Res.* 6 (2015) 571–577.
- [6] V. Blasucci, R. Hart, V.L. Mestre, D.J. Hahne, M. Burlager, H. Huttenhower, B.J.R. Thio, P. Pollet, C.L. Liotta, C.A. Eckert, Single component, reversible ionic liquids for energy applications, *Fuel* 89 (2010) 1315–1319.
- [7] M.S. Shannon, J.E. Bara, Reactive and reversible ionic liquids for CO₂ capture and acid gas removal, *Sep. Sci. Technol.* 47 (2012) 178–188.
- [8] D. Madden, T. Curtin, J.P. Hanrahan, J. Tobin, CO₂ sorption performance by aminosilane functionalized spheres prepared via co-condensation and post-synthesis methods, *AIChE J.* 62 (2016) 2825–2832.
- [9] M. Gonzalez-Miquel, M. Talreja, A.L. Ethier, K. Flack, J.R. Switzer, E.J. Biddinger, P. Pollet, J. Palomar, F. Rodriguez, C.A. Eckert, C.L. Liotta, COSMO-RS studies: structure–property relationships for CO₂ capture by reversible ionic liquids, *Ind. Eng. Chem. Res.* 51 (2012) 16066–16073.
- [10] C.-H. Huang, W. Klinthong, C.-S. Tan, SBA-15 grafted with 3-aminopropyl triethoxysilane in supercritical propane for CO₂ capture, *J. Supercrit. Fluids* 77 (2013) 117–126.
- [11] W. Klinthong, C.-H. Huang, C.-S. Tan, CO₂ capture by mesoporous SBA-15 grafted with 3-aminopropyl triethoxysilane in supercritical propane, *Energy Procedia* 37 (2013) 175–179.
- [12] S. Paul, A.K. Ghoshal, B. Mandal, Kinetics of absorption of carbon dioxide into aqueous blends of 2-(1-piperazinyl)-ethylamine and N-methyldiethanolamine, *Chem. Eng. Sci.* 64 (2009) 1618–1622.
- [13] M. Afkhamipour, M. Mofarahi, Comparison of rate-based and equilibrium-stage models of a packed column for post-combustion CO₂ capture using 2-amino-2-methyl-1-propanol (AMP) solution, *Int. J. Greenh. Gas Control* 15 (2013) 186–199.
- [14] J.-J. Ko, M.-H. Li, Kinetics of absorption of carbon dioxide into solutions of N-methyldiethanolamine+water, *Chem. Eng. Sci.* 55 (2000) 4139–4147.
- [15] M.M. Ghiasi, A. Hajinezhad, H. Yousefi, A.H. Mohammadi, CO₂ loading capacity of DEA aqueous solutions: modeling and assessment of experimental data, *Int. J. Greenh. Gas Control* 56 (2017) 289–301.
- [16] S.N. Khan, S.M. Hailegiorgis, Z. Man, A.M. Shariff, S. Garg, Thermophysical properties of aqueous N-methyldiethanolamine (MDEA) and ionic liquids 1-butyl-3-methylimidazolium trifluoromethanesulfonate [bmim][OTf], 1-butyl-3-methylimidazolium acetate [bmim][Ac] hybrid solvents for CO₂ capture, *Chem. Eng. Res. Des.* 121 (2017) 69–80.
- [17] G. Murshid, W. Ahmad Butt, S. Garg, Investigation of thermophysical properties for aqueous blends of sarcosine with 1-(2-aminoethyl) piperazine and diethylenetriamine as solvents for CO₂ absorption, *J. Mol. Liq.* 278 (2019) 584–591.
- [18] S. Garg, A.M. Shariff, M.S. Shaikh, B. Lal, A. Aftab, N. Faiqa, Selected physical properties of aqueous potassium salt of l-phenylalanine as a solvent for CO₂ capture, *Chem. Eng. Res. Des.* 113 (2016) 169–181.
- [19] S. Garg, A.M. Shariff, M.S. Shaikh, B. Lal, A. Aftab, N. Faiqa, Measurement and prediction of physical properties of aqueous sodium salt of l-phenylalanine, *J. Serb. Chem. Soc.* 82 (2016) 905–919.
- [20] E. Álvarez, D. Gómez-Díaz, M.D. La Rubia, J.M. Navaza, Densities and viscosities of aqueous ternary mixtures of 2-(Methylamino)ethanol and 2-(Ethylamino)ethanol with diethanolamine, triethanolamine, n-methyldiethanolamine, or 2-amino-1-methyl-1-propanol from 298.15 to 323.15 K, *J. Chem. Eng. Data* 51 (2006) 955–962.

- [21] S. Garg, G. Murshid, F.S. Mjalli, W. Ahmad, Physical properties of aqueous blend of diethanolamine and sarcosine: experimental and correlation study, *Chem. Pap.* 71 (2017) 1799–1807.
- [22] M.S. Shaikh, A.M. Shariff, S. Garg, M.A. Bustam, Physical properties of aqueous solutions of potassium L-prolinate from 298.15 to 343.15 K at atmospheric pressure, *Chem. Pap.* 71 (2017) 1185–1194.
- [23] S. Balchandani, B. Mandal, S. Dharaskar, Measurements and modeling of vapor liquid equilibrium of CO₂ in amine activated imidazolium ionic liquid solvents, *Fluid Phase Equilib.* 521 (2020) 112643.
- [24] S. Balchandani, B. Mandal, S. Dharaskar, A. Kumar, S. Bandyopadhyay, Thermally induced characterization and modeling of physicochemical, acoustic, rheological, and thermodynamic properties of novel blends of (HEF + AEP) and (HEF + AMP) for CO₂/H₂S absorption, *Environ. Sci. Pollut. Res.* 26 (2019) 32209–32223.
- [25] D. Li, J. Wang, Y. Gao, X. Zhan, M. Li, Y. Wang, Density, viscosity, and refractive index of binary mixtures of fatty acid ethyl Esters with ethylcyclohexane, *J. Chem. Eng. Data* 64 (2019) 5324–5331.
- [26] B.P. Mandal, M. Kundu, S.S. Bandyopadhyay, Density and viscosity of aqueous solutions of (N-methyldiethanolamine + monoethanolamine), (N-methyldiethanolamine + diethanolamine), (2-amino-2-methyl-1-propanol + monoethanolamine), and (2-amino-2-methyl-1-propanol + diethanolamine), *J. Chem. Eng. Data* 48 (2003) 703–707.
- [27] S. Garg, A.M. Shariff, M.S. Shaikh, B. Lal, H. Suleman, N. Faiqa, Experimental data, thermodynamic and neural network modeling of CO₂ solubility in aqueous sodium salt of L-phenylalanine, *J. CO₂ Util.* 19 (2017) 146–156.
- [28] A. Ali, A. Abdulrahman, S. Garg, K. Maqsood, G. Murshid, Application of artificial neural networks (ANN) for vapor-liquid-solid equilibrium prediction for CH₄-CO₂ binary mixture, *Greenhouse Gas. Sci. Technol.* 0 (2018).
- [29] M.S. Shaikh, A.M. Shariff, M.A. Bustam, S. Garg, K. Qureshi, P.H. Shaikh, I. Bhatti, Experimental studies and artificial neural network modeling of surface tension of aqueous sodium L-prolinate solutions and piperazine blends, *Chin. J. Chem. Eng.* (2019) <https://doi.org/10.1016/j.cjche.2019.01.006>.
- [30] M.A. Sedghamiz, A. Rasoolzadeh, M.R. Rahimpour, The ability of artificial neural network in prediction of the acid gases solubility in different ionic liquids, *J. CO₂ Util.* 9 (2015) 39–47.
- [31] M.E. Hamzehie, M. Fattahi, H. Najibi, B. Van der Bruggen, S. Mazinani, Application of artificial neural networks for estimation of solubility of acid gases (H₂S and CO₂) in 32 commonly ionic liquid and amine solutions, *J. Nat. Gas Sci. Eng.* 24 (2015) 106–114.
- [32] G.F. Versteeg, W.P.M. Van Swaaij, Solubility and diffusivity of acid gases (carbon dioxide, nitrous oxide) in aqueous alkanolamine solutions, *J. Chem. Eng. Data* 33 (1988) 29–34.
- [33] L. Li, J. Zhang, Q. Li, B. Guo, T. Zhao, F. Sha, Density, viscosity, surface tension, and spectroscopic properties for binary system of 1,2-ethanediamine+diethylene glycol, *Thermochim. Acta* 590 (2014) 91–99.